2015

A Mathematical Model of Idiopathic Pulmonary Fibrosis

Wenrui Hao

Clay Marsh

Avner Friedman

PLOS | ONE

RESEARCH ARTICLE

A Mathematical Model of Idiopathic Pulmonary Fibrosis

Wenrui Hao[1]*, Clay Marsh[2], Avner Friedman[3]

1 Mathematical Biosciences Institute, The Ohio State University, Columbus, OH, United States of America, **2** Health Sciences Center South, West Virginia University, Morgantown, WV, United States of America, **3** Mathematical Biosciences Institute & Department of Mathematics, The Ohio State University, Columbus, OH, United States of America

* hao.50@mbi.osu.edu

Citation: Hao W, Marsh C, Friedman A (2015) A Mathematical Model of Idiopathic Pulmonary Fibrosis. PLoS ONE 10(9): e0135097. doi:10.1371/journal.pone.0135097

Editor: Qiang Ding, univeristy of alabama at birmingham, UNITED STATES

Received: April 14, 2015

Accepted: July 16, 2015

Published: September 8, 2015

Data Availability Statement: All relevant data are within the paper.

Funding: This research has been supported by the Mathematical Biosciences Institute and the National Science Foundation under Grant DMS 0931642 (http://nsf.gov/awardsearch/showAward?AWD_ID = 0931642).

Competing Interests: The authors have declared that no competing interests exist.

Abstract

Idiopathic pulmonary fibrosis (IPF) is a disease of unknown etiology, and life expectancy of 3-5 years after diagnosis. The incidence rate in the United States is estimated as high as 15 per 100,000 persons per year. The disease is characterized by repeated injury to the alveolar epithelium, resulting in inflammation and deregulated repair, leading to scarring of the lung tissue, resulting in progressive dyspnea and hypoxemia. The disease has no cure, although new drugs are in clinical trials and two agents have been approved for use by the FDA. In the present paper we develop a mathematical model based on the interactions among cells and proteins that are involved in the progression of the disease. The model simulations are shown to be in agreement with available lung tissue data of human patients. The model can be used to explore the efficacy of potential drugs.

Introduction

Idiopathic pulmonary fibrosis (IPF) is a disease in which scar tissue in the lung is deposited; the deposition of the scar tissue is called fibrosis. As the disease progresses, alveolar-capillary units are impacted, oxygen and carbon dioxide exchange is impaired, ultimately leading to respiratory failure. IPF usually affects older people [1], but its etiology is unknown. IPF has no cure yet, and life expectancy is 3-5 years after diagnosis [2]. IPF is characterized by repeated injury to alveolar epithelium. The injury results in loss of alveolar epithelial cells (AECs) due to increased apoptosis, epithelial to mesenchymal transition (EMT), and abnormal tissue repair [3]. Oxidative stress is associated with the disregulation of the AECs [4, 5], and inflammation is initiated by damaged AECs [6]. Fibrocytes, bone marrow mesenchymal progenitor cells circulating in the blood, play a role in wound repair and are increased in lungs of patients with IPF. However, fibrocyte numbers do not correlate with disease severity [7, 8].

Inflammation and injury activate AECs [9, 10, 11], and activated AECs secrete a number of pro-inflammatory mediators including tumor necrotic factor alpha (TNF-α) [12, 13] and chemoattractant monocyte chemotactic protein-1 (MCP-1) [7, 14, 15]. MCP-1 recruits circulating monocytes from the blood into damaged lung tissue, where they differentiate into classically

activated macrophages M1.In normal lung tissue (homeostasis), macrophages from blood monocytes develop into alveolar macrophages (AM) [12, 16]. Alveolar macrophages are often referred to as alternatively activated macrophages, or M2 macrophages. However M2 macrophages are heterogeneous, and in IPF there appears to be a shift from monocyte-derived M1 macrophages to pro-fibrotic M2 macrophages [17, 18]. These M2 macrophages are responsible for the progression from inflammation to interstitial fibrosis [2, 18] by secreting platelet-derived growth factor (PDGF) [19, 17], transforming growth factor-beta (TGF-β) [17], matrix metalloproteinase (MMP) and tissue inhibitor of metalloproteinase (TIMP) [17], all of which are involved in the regulation of tissue fibrosis. TGF-β is produced also by fibroblasts activated by AEC [12, 20]. Both TGF-β and reactive oxygen species increase AEC apoptosis [20].

TNF-α is produced by the proinflammatory macrophages as well as by activated AEC, and it induces polarization of M2 into M1 [21] which helps to resolve the fibrosis. This polarization by TNF-α is resisted by IL-13 [22, 23, 24] which is produced by M2 macrophages and TH2 lymphocytes [25]. On the other hand, MMP28 [26] and other extracellular matrix (ECM) molecules (e.g. monomeric collagen type 1 interacting with CD204 on M1 [17]) activate polarization of M1 into M2 macrophages. TGF-β, along with AEC-derived basic fibroblast growth factor (bFGF) increase the proliferation of interstitial fibroblasts [6, 20]. PDGF and TGF-β transform fibroblasts into myofibroblasts [27, 28, 29, 30], which together with fibroblasts produce ECM. Imbalance between MMP and its inhibitor TIMP facilitates the accumulation of ECM and the formation of fibrosis [31].

Fibrosis is a disease in which scar tissue develops in an organ resulting in loss of functionality of the organ. Although this process evolves in nearly identical way in all organs, there may be some aspects which are organ specific. Recently Hao et. al. [32] developed a mathematical model of renal interstitial fibrosis and demonstrated that the model can be used to monitor the effect of treatment by anti-fibrotic drugs that are currently being used, or undergoing clinical trials, in non-renal fibrosis. The present paper is based on the model developed in [32] but in addition in includes two features that are unique to pulmonary fibrosis. The first one is the fact that in lung fibrosis we need to deal with two phenotypes of macrophages: monocyte-derived inflammatory macrophages (M1) and anti-inflammatory alveolar macrophages (M2). The network shown in Fig 1 is similar to the network in Fig 1 of [32], but in the present figure the macrophages are divided into M1 and M2 phenotypes, and they play different roles in the fibrotic process.

The second unique feature in lung fibrosis is the geometry of the lung which includes a very large number of alveoli. This complex geometry is represented, in a simplified form, in Fig 2. Our mathematical model of IPF is based on Fig 1 combined with 'homogenization' method associated with Fig 2.

The present paper develops for the first time a mathematical model of IPF. The model is based on the experimental and clinical information referenced above, schematically summarized in the network shown in Fig 1. The model is represented by a system of partial differential equations. The model is validated by comparing the simulation results with patients data and may be used to test the efficacy of potential drugs in stopping the patient's growth of fibrosis.

Materials and Methods

Mathematical model

Table 1 lists all the variables of the model in units of g/cm^3. For the purpose of mathematical modeling we use a simple representation of the lung geometry, whose 2-dimensional projection is shown in Fig 2. The tissue under consideration is a cube R with edge-size 1 cm. The cube is partitioned by periodically arranged small cubes T_ε with edge-size ε, and in each ε-cube there

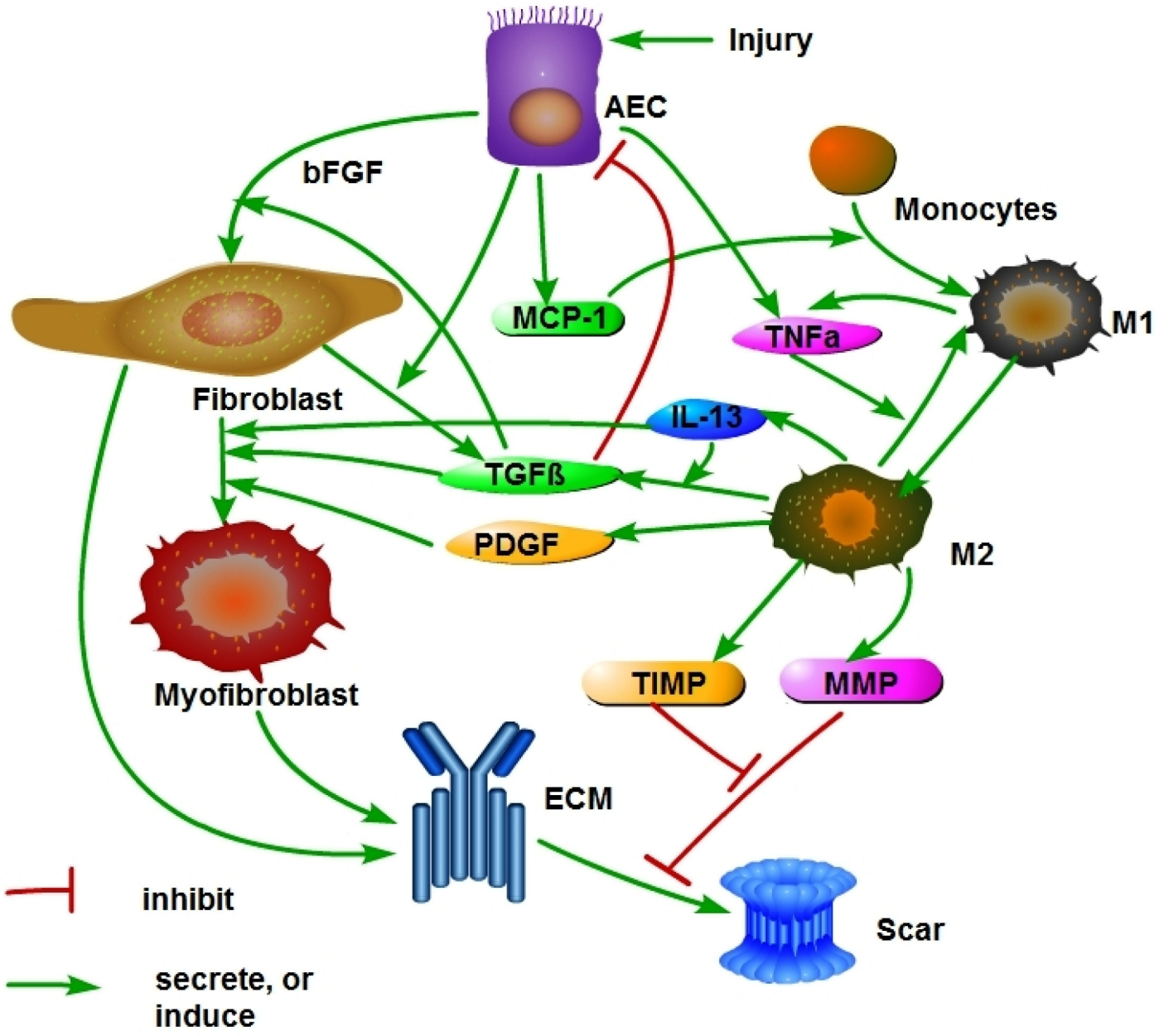

Fig 1. Schematic network of cells and proteins in IPF.

doi:10.1371/journal.pone.0135097.g001

is a concentric cube A_ε of edge-size $(1-\theta)\varepsilon$; the A_ε represent the alveoli air space, and the domains $T_\varepsilon/A_\varepsilon$ represent the alveolar tissue. An alveolar diameter is approximately 140 μm [33] and the thickness of the arterial wall which contains the capillaries, epithelial cells and fibroblasts is 10 μm. We correspondingly take $\frac{1-\theta}{\theta} = 6$, i.e., $\theta = 1/7$. The dimensions of a lung are $12 \times 31 \times 41\ cm^3$, and there are approximately 350 million alveoli in a lung. Hence ε is extremely small.

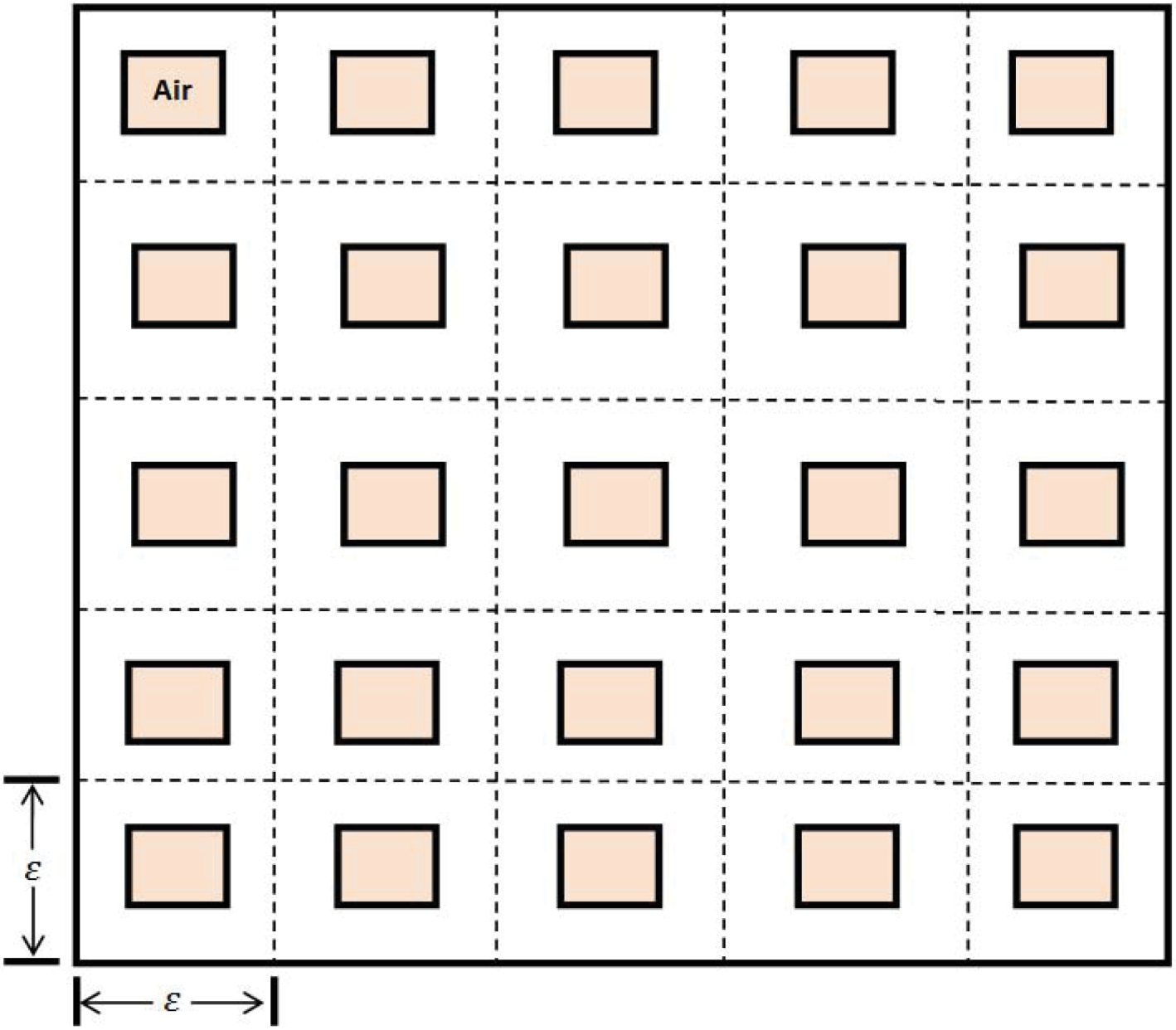

Fig 2. Lung geometry consists of a periodically arranged cubes with smaller cubes representing the air space of alveoli.

doi:10.1371/journal.pone.0135097.g002

We first write down all the differential equation in $T_\varepsilon/A_\varepsilon$, and then take $\varepsilon \to 0$ to obtain the homogenized system in the cube R. The variables that will be used in the model are given in Table 1.

Equation for macrophage density. The equation for macrophage density in $T_\varepsilon/A_\varepsilon$ (coming from the blood) is given by

$$\frac{\partial M_1}{\partial t} - D_M \nabla^2 M_1 = \underbrace{-\nabla \cdot (M_1 \chi_P \nabla P)}_{chemotaxis} \underbrace{-d_{M1} M_1}_{apoptosis} + \underbrace{\lambda_{MT} \frac{T_\alpha}{K_{T_\alpha} + T_\alpha} M_2}_{M_2 \to M_1} \underbrace{-\lambda_{M1} M_1}_{M_1 \to M_2}.$$

Table 1. The variables of the model in units of g/cm^3.

M_1:	density of M1 macrophages	M_2:	density of M2 macrophages
E_0:	density of AEC	E	density of activated AEC
f:	density of fibroblast	m:	density of myofibroblast
ρ:	density of ECM	P:	concentration of MCP-1
G:	concentration of PDGF	T_β:	concentration of activated TGF-β
Q:	concentration of MMPs	Q_I:	concentration of TIMP
T_α	concentration of TNF-α	I_{13}	concentration of IL-13
S	scar density		

doi:10.1371/journal.pone.0135097.t001

Macrophages are terminally differentiated cells; they do not proliferate. They differentiate from monocytes that are circulating in the blood and are attracted by MCP-1 into the lung tissue. Hence they satisfy the boundary condition

$$D_M \frac{\partial M_1}{\partial n} + \tilde{\beta}(P)(M_0 - M_1) = 0 \text{ on } \partial T_\varepsilon.$$

where $\tilde{\beta}(P)$ depends on MCP-1 concentration, P. Here M_0 denotes the density of monoctyes in the blood, i.e., the source of M_1 macrophages from the vascular system. We note that the above Robin boundary condition arises from boundary homogenization of the vascular system, as done, for example, in [34]. The term $\lambda_{MT}\frac{T_\alpha}{K_{T_\alpha}+T_\alpha}M_2$ accounts for transformation from M2 to M1 induced by TNF-α [21]. The term $-\nabla\cdot(M_1\chi_P\nabla P)$ is the chemotactic effect of MCP-1 on M1 macrophages; χ_P is the chemotactic coefficient. As noted in the Introduction, macrophages from blood monocytes evolve into AM [12, 16] and, in IPF, there is a shift from AM to pro-fibrotic M2 macrophages. There is also a polarization from M1 to M2 induced by MMP28 [26], and by collagen type I via CD204 receptor on M1 [17]. The term $\lambda_{M1}M1$ represents polarization from M1 to M2 by the above processes and possibly other processes (e.g. [35]).

We want replace the boundary condition of M_1, by a spatial distribution f. If $D_M\nabla^2 u = f$ in $T_\varepsilon/A_\varepsilon$, $\frac{\partial u}{\partial n} = 0$ on ∂A_ε, $D_M\frac{\partial u}{\partial n} = g$ on ∂T_ε, then, by integration $\int_{T_\varepsilon/A\varepsilon} f dV = \int_{\partial T_\varepsilon} g dS$. Hence

$$\bar{f} \times \text{volume of } T_\varepsilon/A_\varepsilon = \bar{g} \times \text{area of } \partial T_\varepsilon,$$

where $\bar{f}$ and $\bar{g}$ are the mean values of f and g. Since

$$\text{volume of } T_\varepsilon/A_\varepsilon = \varepsilon^3[1-(1-\theta)^3] = \gamma\varepsilon^2, \quad \text{area of } \partial T_\varepsilon = 6\varepsilon^2,$$

where $\gamma = 127/343$, and ε is small so that $\bar{f} \approx f$ and $\bar{g} \approx g$, we can replace the boundary condition of $M1$ by the spatial distribution $6\varepsilon\tilde{\beta}(P)/\gamma = \beta(P)$. Hence, the equation for M1 density in $T_\varepsilon/A_\varepsilon$ is given by

$$\begin{aligned} \frac{\partial M_1}{\partial t} - D_M\nabla^2 M_1 &= \beta(P)(M_0 - M_1) - \nabla\cdot(M_1\chi_P\nabla P) - d_{M1}M_1 \\ &\quad + \lambda_{MT}\frac{T_\alpha}{K_{T_\alpha}+T_\alpha}M_2 - \lambda_{M1}M_1, \end{aligned} \tag{1}$$

with zero boundary flux. We take $\beta(P) = \beta\frac{P}{K_P+P}$, where β is a constant

The M2 macrophage density satisfies the equation

$$\frac{\partial M_2}{\partial t} - D_M \nabla^2 M_2 = \underbrace{\lambda_{M1} M_1}_{M_1 \to M_2} \underbrace{-d_{M2} M_2}_{apoptosis} \underbrace{-\lambda_{MT} \frac{T_\alpha}{K_{T_\alpha} + T_\alpha} M_2}_{M_2 \to M_1}, \tag{2}$$

where the first and last terms on the right-hand side are complimentary to the corresponding terms in Eq (1).

Equation for AEC density (E_0 and E). The equation of the inactivated AEC density is given by

$$\frac{dE_0}{dt} = A_{E_0} \left(1 + \underbrace{\frac{\lambda_1 E_0 I_D}{K_D + E_0 I_D}}_{repair} \right) \underbrace{-d_{E_0} E_0 \left(1 + \delta + d_{E_0 T} \frac{T_\beta}{K_{T_\beta} + T_\beta} \right)}_{apoptosis} \underbrace{-\lambda_{E_0} E_0 I_D}_{E_0 \to E}. \tag{3}$$

In normal healthy, the production of E_0 is represented by the term A_{E_0} and the death rate is represented by $d_{E0}E_0$.

The equation for the activated AEC is

$$\frac{dE}{dt} = \underbrace{\lambda_{E_0} E_0 I_D}_{activation} \underbrace{-\lambda_{EM} E I_D}_{EMT} \underbrace{-d_E E}_{apoptosis}. \tag{4}$$

In homeostasis, $I_D = \emptyset$, $\delta = 0$ and activated TGF-β concentration is very small. The injury to the epithelium is expressed in two ways: (i) by activation of AEC, which is represented by term $\lambda_{E_0} E_0 I_D$, where D is the damaged region and $I_D = 1$ on D and $I_D = 0$ elsewhere, and (ii) by increased apoptosis caused by oxidative stress [4, 5] (the term δ) and by TGF-β [20, 3]. In IPF, the damaged epithelium is partially repaired by fibrocytes, and this is expressed by the term $\frac{\lambda_1 E_0 I_D}{K_D + E_0 I_D}$ [7]. The second term of the right-hand side in Eq (4) accounts for EMT due to injury [3].

Equations for fibroblast density (f) and myofibroblast density (m). The fibroblasts and myofibroblasts equations are given by:

$$\begin{aligned} \frac{\partial f}{\partial t} - D_f \nabla^2 f = {} & \underbrace{\lambda_{Ef} E_0}_{source} + \underbrace{\lambda_{fE} \left(\frac{T_\beta}{K_{T_\beta} + T_\beta} + \frac{I_{13}}{K_{I_{13}} + I_{13}} \right) \frac{E}{K_E + E} f}_{production} \underbrace{-d_f f}_{apoptosis} \\ & \underbrace{- \left(\lambda_{mfT} \frac{T_\beta}{K_{T_\beta} + T_\beta} + \lambda_{mfG} \frac{G}{K_G + G} \right) f}_{f \to m}, \end{aligned} \tag{5}$$

$$\frac{\partial m}{\partial t} - D_m \nabla^2 m = \underbrace{\left(\lambda_{mfT} \frac{T_\beta}{K_{T_\beta} + T_\beta} + \lambda_{mfG} \frac{G}{K_G + G} \right) f}_{f \to m} \underbrace{-d_m m}_{apoptosis}. \tag{6}$$

The first term on the right-hand side of Eq (5) is a source from E_0-derived bFGF, which for simplicity we take to be in the form $\lambda_{Ef} E_0$. As in [32], TGF-β and PDGF transform fibroblasts into myofibroblasts [27, 28, 29, 30]. Furthermore, TGF-β and IL-13 [22, 23, 24], along with E-derived bFGF, increase proliferation of fibroblasts [6, 32, 27]. For simplicity, we do not include bFGF specifically in the model, but instead represent it by E. The production of fibroblasts in

healthy normal tissue depends on the density of AECs in homeostasis, and is represented by the term $\lambda_{Ef}E_0$ [6, 20].

Equation for ECM density (ρ) and scar (S). The ECM, produced by fibroblasts and myofibroblasts [27, 28, 29, 30], is degraded by MMP [36], and TGF-β enhances the production of ECM by myofibroblasts [27, 28, 29, 30]. The equation for the density of ECM is then given (as in [32]) by:

$$\frac{\partial \rho}{\partial t} = \underbrace{\lambda_{\rho f} f\left(1-\frac{\rho}{\rho_0}\right)^+ + \lambda_{\rho m}\left(1+\lambda_{\rho T_\beta}\frac{T_\beta}{K_{T_\beta}+T_\beta}\right)m}_{production} \underbrace{-d_\rho \rho - d_{\rho Q} Q\rho}_{degradation}, \tag{7}$$

where $\left(1-\frac{\rho}{\rho_0}\right)^+ = 1-\frac{\rho}{\rho_0}$ if $\rho < \rho_0$, $\left(1-\frac{\rho}{\rho_0}\right)^+ = 0$ if $\rho \geq \rho_0$.

Excessive accumulation of ECM components (particularly collagen) associated with tissue injury and inflammation, results in permanent scar formation [37]. Within each type of scar, there is considerable heterogeneity: an imbalance between MMP and TIMP activity has been implicated in the development of scar [31]. Thus a scar depends on production and deposition of ECM and disruption of normal, healthy protein cross-linking. We define the scar simply by the equation

$$S = \lambda_S(\rho-\rho^*)^+, \tag{8}$$

where ρ^* is the ECM density in homeostasis and λ_S is a constant, but this definition is a simplified characterization of a scar since it does not account for disruption in protein cross-linking.

Equation for MCP-1 (P). The MCP-1 equation is given by

$$\frac{\partial P}{\partial t} - D_P\nabla^2 P = \underbrace{\lambda_{PE}E}_{production} \underbrace{-d_P P - d_{PM}\frac{P}{K_P+P}M_1}_{degradation}, \tag{9}$$

where λ_{PE} represents the growth rate by activated AEC following damage to the endothelium [32, 7, 14, 15, 1]. The last term accounts for the internalization of MCP-1 by macrophage, which may be limited due to the limited rate of receptor recycling.

Equations for concentrations of PDGF (G), MMP (Q), TIMP (Q_r), TGF-β (T_β), TNF-α (T_α) and IL-13 (I_{13}). As in [32], the following sets of diffusion equations hold for G, Q and Q_r:

$$\frac{\partial G}{\partial t} - D_G\nabla^2 G = \underbrace{\lambda_{GM}M_2}_{production} \underbrace{-d_G G}_{degradation}, \tag{10}$$

$$\frac{\partial Q}{\partial t} - D_Q\nabla^2 Q = \underbrace{\lambda_{QM}M_2}_{production} \underbrace{-d_{QQ_r}Q_r Q}_{depletion} \underbrace{-d_Q Q}_{degradation}, \tag{11}$$

$$\frac{\partial Q_r}{\partial t} - D_{Q_r}\nabla^2 Q_r = \underbrace{\lambda_{Q_rM}M_2}_{production} \underbrace{-d_{Q_rQ}QQ_r}_{depletion} \underbrace{-d_{Q_r}Q_r}_{degradation}. \tag{12}$$

Note that in Eq (11), MMP is lost by binding with TIMP (second term).

As in [32], TGF-β is produced and activated by M2 macrophages while enhanced by IL-13 [22, 23, 24]; in addition, TGF-β is produced and activated by fibroblasts and AEC [12, 20]:

$$\frac{\partial T_\beta}{\partial t} - D_{T_\beta}\nabla^2 T_\beta = \underbrace{\lambda_{T_\beta M} M_2\left(1+\lambda_{T_\beta I_{13}}\frac{I_{13}}{I_{13}+K_{I_{13}}}\right)+\lambda_{T_\beta f} f\frac{E}{E+K_E}}_{production}\ \underbrace{-d_{T_\beta}T_\beta}_{degradation}. \quad (13)$$

TNF-α is produced by M1 macrophages [21], and is also produced by AEC [12, 13]:

$$\frac{\partial T_\alpha}{\partial t} - D_{T_\alpha}\nabla^2 T_\alpha = \underbrace{\lambda_{T_\alpha M} M_1+\lambda_{T_\alpha E}E}_{production}\ \underbrace{-d_{T_\alpha}T_\alpha}_{degradation}\ \underbrace{-\lambda_{MT_\alpha}\frac{T_\alpha}{K_{T_\alpha}+T_\alpha}M_2}_{M_2\to M_1}. \quad (14)$$

IL-13 is produced by M2 macrophages [22, 23], and follows the equation

$$\frac{\partial I_{13}}{\partial t} - D_{I_{13}}\nabla^2 I_{13} = \underbrace{\lambda_{I_{13}}+\lambda_{I_{13}M}M_2}_{production}\ \underbrace{-d_{I_{13}}I_{13}}_{degradation}. \quad (15)$$

Actually, IL-13 is also produced by TH2 cells [25]; for simplicity we do not include TH2 cells in our model but accounts for their production of IL-13 by the term $\lambda_{I_{13}}$.

The homogenized equations. On the boundary of $T_\varepsilon/A_\varepsilon$ all the variables are assumed to have zero flux. Hence, each of the Eqs (1)–(14), if written in the form

$$\frac{\partial X}{\partial t} - D_X\nabla^2 X = F_X(X) \text{ in } T_\varepsilon/A_\varepsilon, \quad (16)$$

takes, after homogenization [38] (Sec. 3.1 and p.31), the following form:

$$\gamma\frac{\partial X}{\partial t} - D_X\tilde{\nabla}^2 X = \gamma F_X(X) \text{ in the cube } R, \quad (17)$$

where γ is the volume fraction of the tissue in each ε-cube, $\gamma = \frac{127}{343}$. Here $\tilde{\nabla}^2 = \sum a_{ij}\frac{\partial^2}{\partial x_i \partial x_j}$, where the coefficient a_{ij} are computed by

$$a_{ij} = \int_{y\in T/A}\left(\delta_{ij}+\frac{\partial \chi_j}{\partial x_i}\right)dy.$$

where χ_i satisfies the equation

$$\nabla^2\chi_i = 0 \text{ in } T\setminus A, \text{ with } \frac{\partial \chi_i}{\partial n}+n_i = 0 \text{ on the boundary of } A;$$

here $T = \frac{T_\varepsilon}{\varepsilon}$, $A = \frac{A_\varepsilon}{\varepsilon}$, n_i is the i-th component of the outward normal n, and χ_i is periodic in the directions of the three axes x_j (j = 1,2,3). Computing a_{ij} by finite element discretization, we find (similarly to [32]) that $a_{ii} = 0.11$ (i = 1,2,3) and $a_{ij} = 0$ if $i \neq j$.

Boundary conditions

All variables are assumed to satisfy the zero flux boundary condition on ∂R, the boundary of the cube R.

Initial conditions

We assume initial homeostasis, that is, $\lambda_{E_0} E_0 I_D = 0$, but with a small amount of inflammation, represented by the term $\lambda_{PE} E$ in Eq (9). We take this term to be 10^{-10} and compute the initial values by solving the steady state equations.

In particular we find the initial values of $T_\alpha = 2.5 \times 10^{-8}$, $T_\beta = 2.51 \times 10^{-12}$ and $I_{13} = 3.2 \times 10^{-8}$ in units of *gm/ml*. Taking into account that only γ-fraction of the space is occupied by tissue, the values $\frac{1}{\gamma} T_\alpha, \frac{1}{\gamma} I_{13}$ coincide with the concentration of T_α and I_{13} measured in the bronchial tubes of healthy lung in [39], and $\frac{1}{\gamma} T_\beta$ coincides with value of TGF-β as computed in [40].

We also compute that $E_0 = E^* = 0.79\ g/cm^3$, $f = f^* = 4.75 \times 10^{-3}\ g/cm^3$, $\rho = \rho^* = 3.26 \times 10^{-3}\ g/cm^3$ and $I_{13} = 1.76 \times 10^{-8}\ g/cm^3$ at $t = 0$.

Results

Numerical scheme

We briefly describe the technique used in the simulations, and for simplicity take R to be the unit cube, i.e., $R = [0, 1] \times [0, 1] \times [0, 1]$. Consider the following general diffusion equation

$$\frac{\partial C}{\partial t} - D_C \nabla^2 C = F_C(C),$$

in R with zero flux on ∂R. Given three positive integers K_1, K_2, K_3, let

$$x_i = i/K_1,\ \ y_j = j/K_2,\ \ z_k = k/K_3,\ \ 0 \le i \le K_1,\ \ 0 \le j \le K_2,\ \ 0 \le k \le K_3.$$

Then we denote $c_{i,j,k}(t)$ the numerical approximation of $C(x_i, y_j, z_k, t)$, and get the following ODE system by semi-discretization:

$$\begin{aligned} \frac{dc_{i,j,k}(t)}{\partial t} &= D_C(K_1^2[c_{i+1,j,k}(t) + c_{i-1,j,k}(t) - 2c_{i,j,k}(t)] + K_2^2[c_{i,j+1,k}(t) + c_{i,j-1,k}(t) - 2c_{i,j,k}(t)] \\ &\quad + K_3^2[c_{i,j,k-1}(t) + c_{i,j,k+1}(t) - 2c_{i,j,k}(t)]) + F_C(c_{i,j,k}(t)). \end{aligned} \tag{18}$$

The Runge-kutta method is employed to solve this ODE system. The above method is used to solve the coupled system of equations of the complete model.

Model simulation and validation

In this section, we simulate the model (1)-(17). The parameter values are listed in Tables 2 and 3 and the initial values are taken as explained above. The numerical simulation were carried out by finite difference scheme in spatial direction and Runge-Kutta method in time direction.

Fig 3 shows the dynamics of the average densities of cells and concentrations of cytokines for 30 days.

Fig 4 shows histogram of cells and cytokines in disease vs. homeostasis. The simulation results for MMP and TIMP shown in Fig 4 are in agreement with the experimental results, reported in [41] for protein concentration human lung tissue with IPF (n = 16 human subjects) and control (n = 6 human subjects). Indeed, although (in [41]) MMP 7 (for IPF) is nearly 4 times the level of MMP7 for control, all other MMPs (1,2,9,13) increased approximately twice or just a little more than twice, while the relatively small concentration of MMP8 decreased to 25% of the control level. The simulation results for TIMP shows an increase of 20% in the protein concentration for IPF vs. control, which is the same as in human lung tissues reported in [41] for TIMP-1,2,3. Levels of mRNA expression relate to levels of the translated proteins. The

Table 2. Parameters' description and value.

Parameter	Description	Value
D_M	dispersion coefficient of macrophages	8.64×10^{-7} cm^2 day^{-1} [32]
D_P	diffusion coefficient of MCP-1	1.728×10^{-1} cm^2 day^{-1} [32]
D_G	diffusion coefficient of PDGF	8.64×10^{-2} cm^2 day^{-1} [32]
D_Q	diffusion coefficient of MMP	4.32×10^{-2} cm^2 day^{-1} [32]
D_{Q_r}	diffusion coefficient for TIMP	4.32×10^{-2} cm^2 day^{-1} [32]
D_{T_β}	diffusion coefficient forTGF-β	4.32×10^{-2} cm^2 day^{-1} [32]
D_{T_α}	diffusion coefficient for TNF-α	1.29×10^{-2} cm^2 day^{-1} [55]
D_f	dispersion coefficient offibroblasts	1.47×10^{-6} cm^2 day^{-1} [32]
D_m	dispersion coefficient of myofibroblasts	1.47×10^{-5} cm^2 day^{-1} [32]
$D_{I_{13}}$	diffusion coefficient of IL-13	1.08×10^{-2} cm^2 day^{-1} [40]
D_{T_α}	diffusion coefficient forTNF-α	1.29×10^{-2} cm^2 day^{-1} [40]
λ_{MT}	transition rate of M2 to M1 macrophages by TNF-α	5×10^{-3} day^{-1} [56]
λ_{M1}	polarization rate of M1 to M2 macrophages	9.02×10^{-6} day^{-1}, estimated
λ_{E_0}	AEC	0.25 day^{-1} estimated
λ_1	repair rate of AEC	10^{-3} g/cm^3 day^{-1} estimated
λ_{EM}	EMT rate of AEC	1.65×10^{-3} day^{-1} estimated
$\lambda_{T_\beta M}$	production rate of TGF-β by macrophages	1.5×10^{-2} day^{-1} [32]
$\lambda_{T_\beta f}$	production rate of TGF-β by fibroblast	7.5×10^{-3} day^{-1} [32] & estimated
λ_{GM}	production rate of PDGF by macrophages	2.4×10^{-5} day^{-1} [32]
λ_{QM}	production rate of MMP by macrophages	3×10^{-4} day^{-1} [32]
$\lambda_{Q,M}$	production rate of TIMP by macrophages	6×10^{-5} day^{-1} [32]
λ_{PE}	activation rate of MCP-1 due to AECs	1×10^{-8} day^{-1} [32]
$\lambda_{\rho f}$	activation rate of ECM due to fibroblasts	3×10^{-3} day^{-1} [32]
$\lambda_{\rho m}$	activation rate of ECM due to myofibroblasts	6×10^{-3} day^{-1} [32]
$\lambda_{\rho T_\beta}$	activation rate of ECM due to TGF-β	2 [32]
λ_{Ef}	activation rate of fibroblasts due to bFGF and TGF-β	2.5×10^{-1} day^{-1} [32] & estimated
λ_{fE}	production rate of fibroblasts	5×10^{-4} day^{-1} [32] & estimated
λ_{mfT}	activation rate of myofibroblasts due to TGF-β	0.12 day^{-1} [32]
λ_{mfG}	activation rate of myofibroblasts due to PDGF	0.12 day^{-1} [32]
$\lambda_{T_\alpha M}$	activation rate of TNF-α due tomacrophage	1.39×10^{-5} day^{-1} [57]
$\lambda_{T_\alpha E}$	activation rate of TNF-α due tomacrophage	6.9×10^{-6} day^{-1} [57] & estimated
$\lambda_{I_{13}}$	production rate of IL-13 by Th2 cells	2.12×10^{-7} g/ml day^{-1} [40]
$\lambda_{I_{13}M}$	production rate of IL-13 by macrophages	3.98×10^{-4} day^{-1} [40]
d_{M_2}	death rate of macrophages	0.015 day^{-1} [32]
d_{M_1}	death rate of macrophages	0.02 day^{-1} [56, 58]
d_E	death rate of AECs	1.65×10^{-2} day^{-1} [32]
d_{E_0}	death rate of AECs	1.65×10^{-2} day^{-1} [32]
d_{E_0T}	death rate of AECs	1.65×10^{-3} day^{-1} [32]
δ	increased death rate of AECs by injury	1×10^{-3} day^{-1}, estimated
d_ρ	degradation rate of ECM	0.37 day^{-1} [32]
d_P	degradation rate of MCP-1	1.73 day^{-1} [32]
d_{PM}	internalization rate of MCP-1 by M1 macrophages	2.08×10^{-4} day^{-1} [32]
d_G	degradation rate of PDGF	3.84 day^{-1} [32]
d_{QQ_r}	binding rate of MMP to TIMP	4.98×10^8 cm^3 g^{-1} day^{-1} [32]
$d_{Q,Q}$	binding rate of TIMP to MMP	1.04×10^9 cm^3 g^{-1} day^{-1} [32]
d_Q	degradation rate of MMP	4.32 day^{-1} [32]
d_{Q_r}	degradation rate of TIMP	21.6 day^{-1} [32]
$d_{\rho Q}$	degradation rate of ECM due to MMP	2.59×10^7 cm^3 g^{-1} day^{-1} [32]
d_{T_β}	degradation rate of TGF-β	3.33×10^2 day^{-1} [32]
d_f	death rate of fibroblasts	1.66×10^{-2} day^{-1} [32]
d_m	death rate of myofibroblasts	1.66×10^{-2} day^{-1} [32]
d_{T_α}	degradation rate of TNF-α	55.45 day^{-1} [59]
$d_{I_{13}}$	degradation rate of IL-13	12.47 day^{-1} [40]

doi:10.1371/journal.pone.0135097.t002

Table 3. Parameters' description and value.

Parameter	Description	Value
χ_P	chemotacticsensitivity parameter by MCP-1	10 $cm^5\ g^{-1}$ day^{-1} [32]
A_{E0}	intrinsic AEC proliferation	8.27×10^{-3} g/cm^3 day^{-1} [32]
K_G	PDGF saturation for activation of myofibroblasts	1.5×10^{-8} gcm^{-3} [32]
K_{T_β}	TGF-β saturation for apoptosis of AECs	1×10^{-10} gcm^{-3} [32]
K_P	MCP-1 saturation for influx of macrophages	5×10^{-9} gcm^{-3} [32]
K_{T_α}	TNF-α saturation	5×10^{-7} gcm^{-3} [40]
$K_{I_{13}}$	IL-13 saturation	2×10^{-7} g/cm^3 [40]
K_E	AEC saturation	0.1 g/cm^3, estimated
ρ_0	ECM saturation	10^{-2} gcm^{-3} [32]
ρ^*	ECM density in health	3.26×10^{-3} gcm^{-3} estimated
E^*	TEC density in health	0.799 gcm^{-3} estimated
f^*	fibroblast density in health	4.75×10^{-3} gcm^{-3} estimated
M_0	source/influx of macrophagesfrom blood	5×10^{-5} gcm^{-3} [32]
β	influx rate of macrophages into interstitium	0.2 cm^{-1} [32]

doi:10.1371/journal.pone.0135097.t003

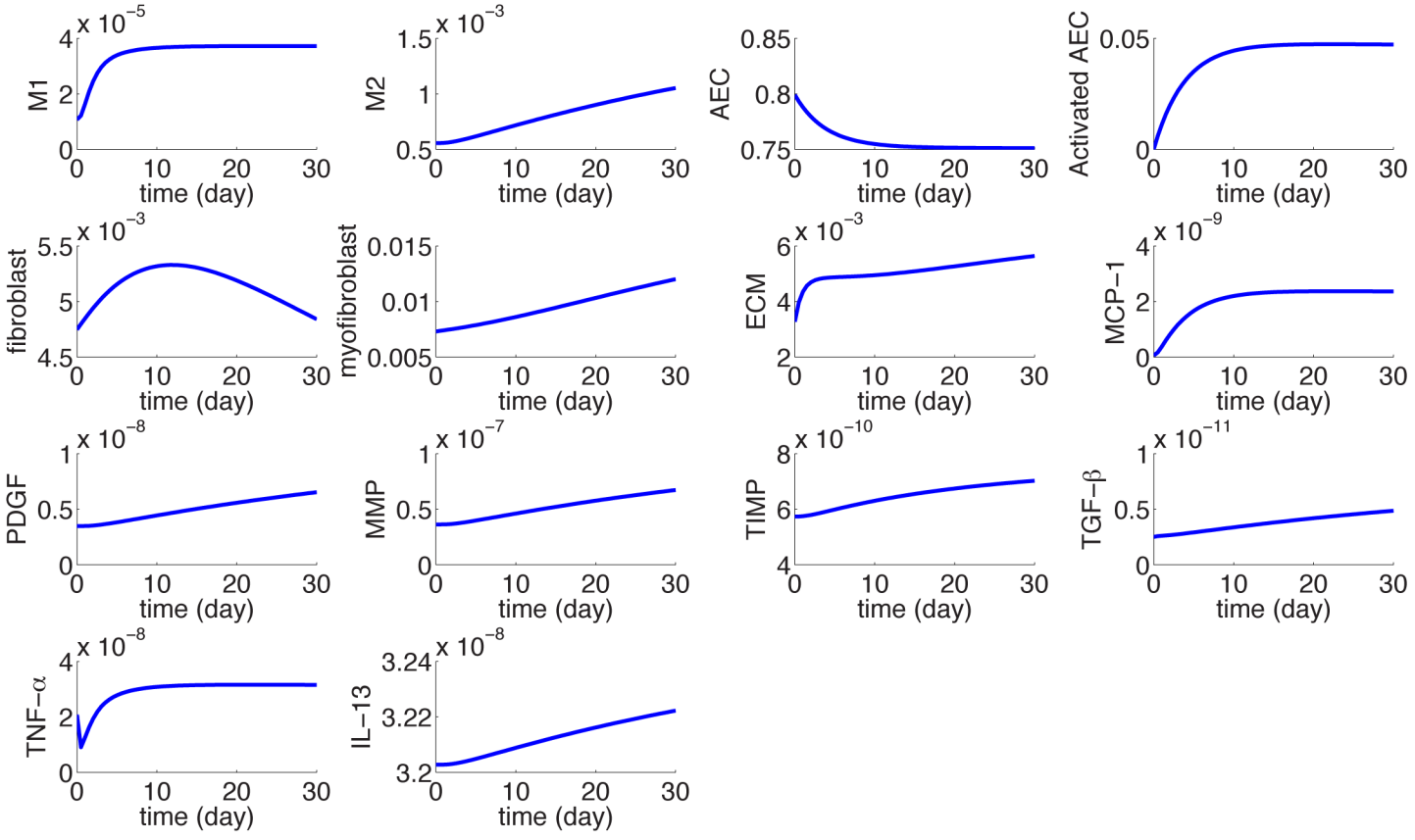

Fig 3. The dynamics of the average concentrations of cells and cytokines in units of gm/cm^3 from homeostasis at day 0 to day 30. l_D = $0.3 \times 0.3 \times 0.3$ cm^3.

doi:10.1371/journal.pone.0135097.g003

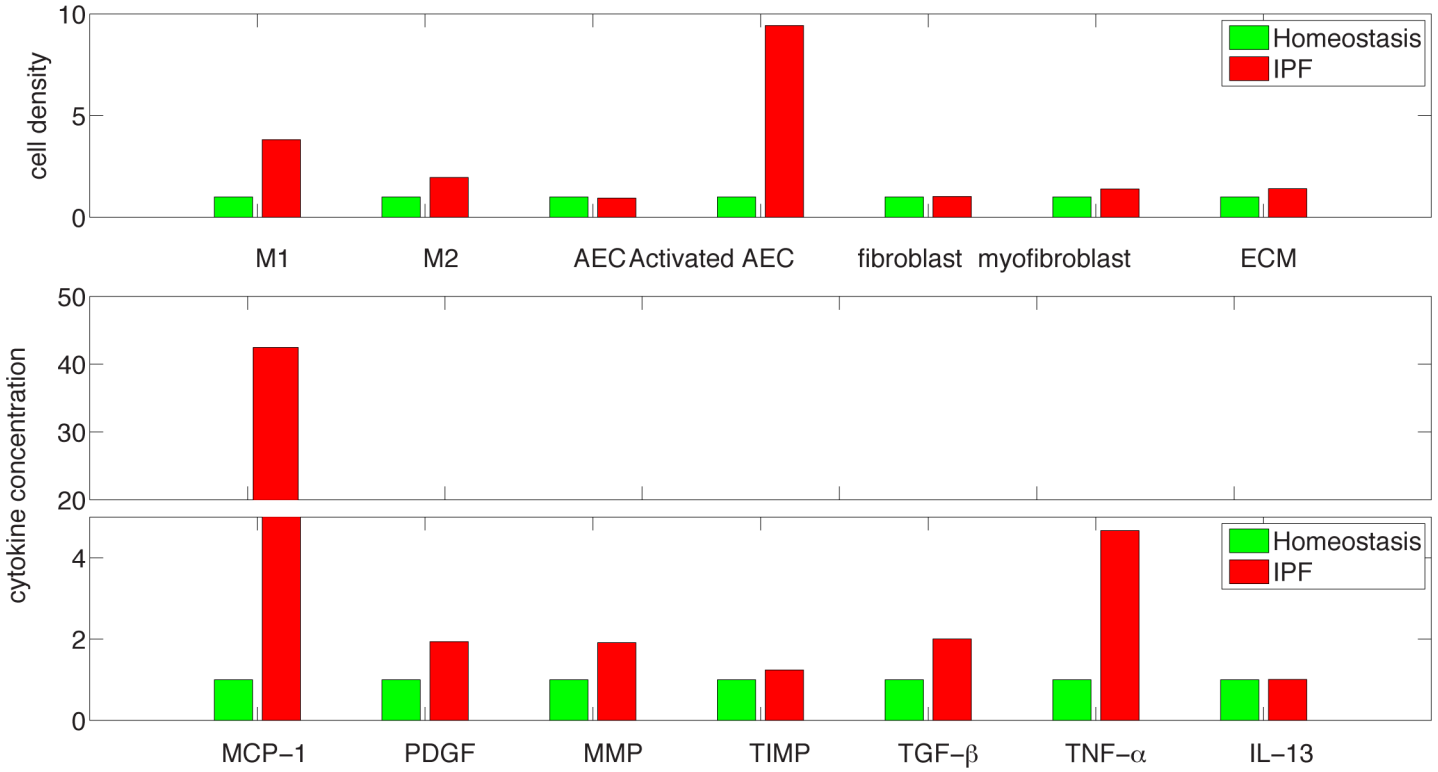

Fig 4. Comparison of cells and cytokines for IPF and healthy control at day 30 from the beginning of the disease (in fraction of healthy control).

doi:10.1371/journal.pone.0135097.g004

mRNA of TGF-β reported in [42] (which can also be deduced from [43]) shows increase by at least twice in IPF vs. control; this increase is the same for the TGF-β protein shown in Fig 4. However, we cannot make too much out of this comparison since TGF-β has to be activated post transcriptionally to be biologically active [20]. The mRNA expressions of TNF-α and PDGF reported in [43] show increased levels in IPF patients, which is in qualitative agreement with the increase in protein levels shown in Fig 4.

Figs 5 and 6 are simulations of the disease for a larger period of 300 days. We see that the disease continue to grow but at slower rate.

Treatment studies

We can use the model to explore potential drugs. Such drugs could be, for instance, anti-TGF-β, anti-PDGF, anti-IL-13 or anti-TNF-α. Fig 7 displays the effect of treatment for mild case of IPF, namely $I_D = 0.3 \times 0.3$ and $\lambda_{E_0} = 2.5 \times 10^{-3}$ day^{-1}, and Fig 8 displays the effect of treatment for severe case of IPF, namely, $I_D = 0.5 \times 0.5$ and $\lambda_{E_0} = 3 \times 10^{-3}$ day^{-1}

Anti TNF-α. To implement the effect of anti-TNF-α (TNF-α receptor that inactivates TNF-α and thus blocks TNF-α activity [44]), we need to modify the model replacing λ_{MT} in Eqs (1) (2) by $\lambda_{MT}/(1 + B_1)$ to represent the inhibition of the activity of TNF-α. We assume that the drug is administered starting at day 100 from the beginning of the disease. The red curve in Figs 7 and 8 show the effect of the drug on the ECM average concentration (with $B_1 = 1$) over a period of 300 days. The corresponding scar has a similar curve and hence it is not

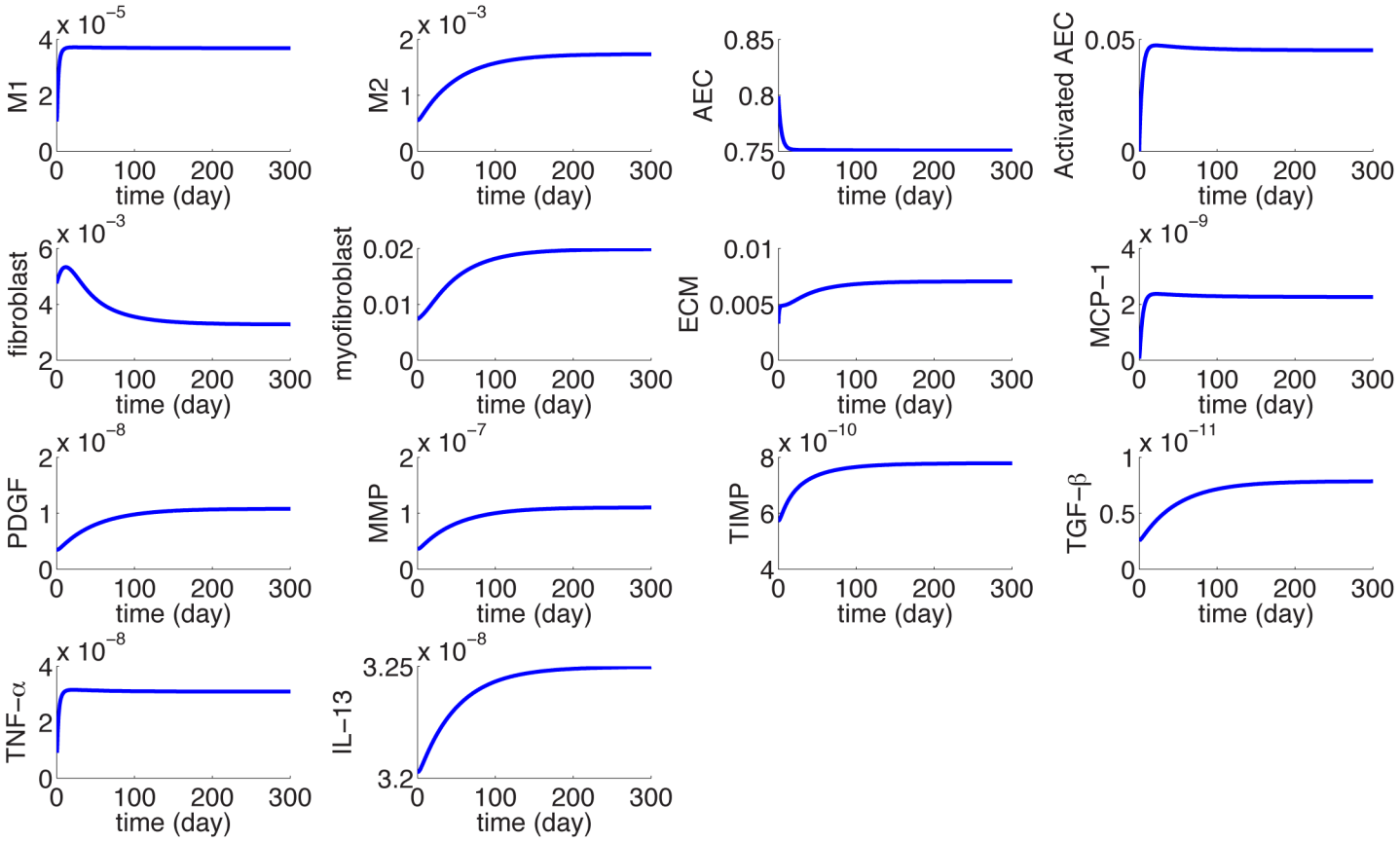

Fig 5. The dynamics of the average concentrations of cells and cytokines in units of gm/cm^3 from homeostasis at day 0 to day 300. $l_D = 0.3 \times 0.3 \times 0.3\ cm^3$.

doi:10.1371/journal.pone.0135097.g005

given here. We see that the drug has no effect on reducing the ECM. This is in agreement with clinical phase 2 trials with Etanercept reported in [44].

The effect of the drug is introduced gradually over a period of 20 days, that is, we actually take $\theta(t)B_1$ instead of B_1, where $\theta(t)$ increases linearly from 0 to 1 over a period of 20 days. The same procedure is used in treatment of the subsequent drugs.

Anti-PDGF. We next consider anti-PDGF treatment, by Imatinib, an inhibitor of PDGFR and thus a blocker of PDGF activity [45]. In our model this corresponds to replacing, in Eqs (5) and (6), λ_{mfG} by $\lambda_{mfG}/(1 + B_2)$. The green curve in Figs 7 and 8 show the effect of the drug on ECM for $B_2 = 1$. We see that the drug does not confer significant benefit, which is in agreement with phase 2 study with Imatinib.

Anti-IL-13. We next consider anti-IL-13, monoclonal antibody, a drug currently in early phase clinical trials. Tralokinamab and lebrikizumab are two drugs delivering antibody that blocks the action of IL-13. To implement their effect in our model we need to replace $\lambda_{T_\beta I_{13}}$ in Eq (13) by $\lambda_{T_\beta I_{13}}/(1 + B_3)$. With the choice of $B_3 = 1$, the blue curve in Figs 7 and 8 show no significant benefits; this seems to suggest that a moderate level of dosing will not be effective.

Anti-TGF-β. We finally consider an anti-TGFβ drug, such as Pirfenidone [46] which was recently approved in the United States. In our model we need to replace $\lambda_{T_\beta M}$ and $\lambda_{T_\beta f}$ by $\lambda_{T_\beta M}/(1 + A)$ and $\lambda_{T_\beta f}/(1 + A)$, and T_β by $T_\beta/(1 + B)$ in all terms where T_β acts to promote fibrosis. In

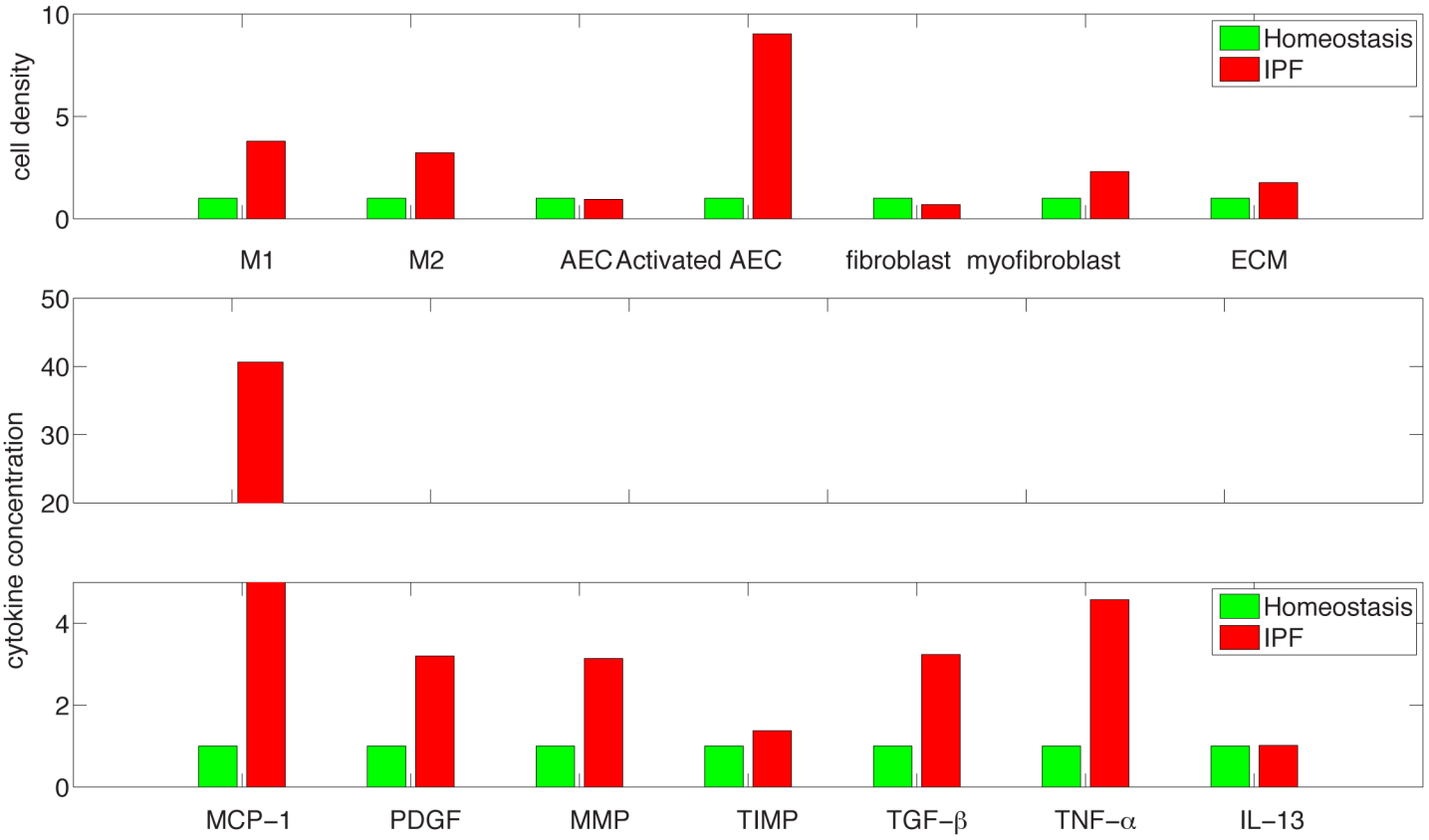

Fig 6. Comparison of cells and cytokines for IPF and healthy control at day 300 from the beginning of the disease (in fraction of healthy control).

doi:10.1371/journal.pone.0135097.g006

the previous examples we showed that the drug has no benfits even at the level $B = 1$. For the present anti-TGF-β drug we demonstrate a clear benefit already with small A and B. Indeed, the cyan curve in Figs 7 and 8 show the effect of the drug on ECM for $A = B = 0.1$. We see that in terms of ECM, the drug could be effective in stopping, or even slowly decreasing fibrosis.

Discussion

IPF is a disease which exhibits, as in cutaneous wounds, both pro-inflammatory features when the alveolar epithelium is damaged and AECs begin to secrete pro-inflammatory mediators, and anti-inflammatory features associated with unsuccessful repair processes.

In this paper we developed for the first time a mathematical model for IPF. The model includes many of the principal players of cells and cytokines associated with the disease. The complex geometry of the lung alveoli is simplified by using the averaging method of homogenization, which provides a way to calculate the effective interactions among the cells and cytokines. The simulations of the model agree with lung tissue data that are available from human patients. The model can be used to explore the effect of drug treatment. Indeed, we used the model to explore the treatment of IPF by anti-TNF-α, anti-PDGF, anti-IL-13 and anti-TGF-β. We found that the first three drugs did not confer any benefits, while the last drug, pirfenidone, could be effective in stopping, or even slowly decreasing fibrosis.

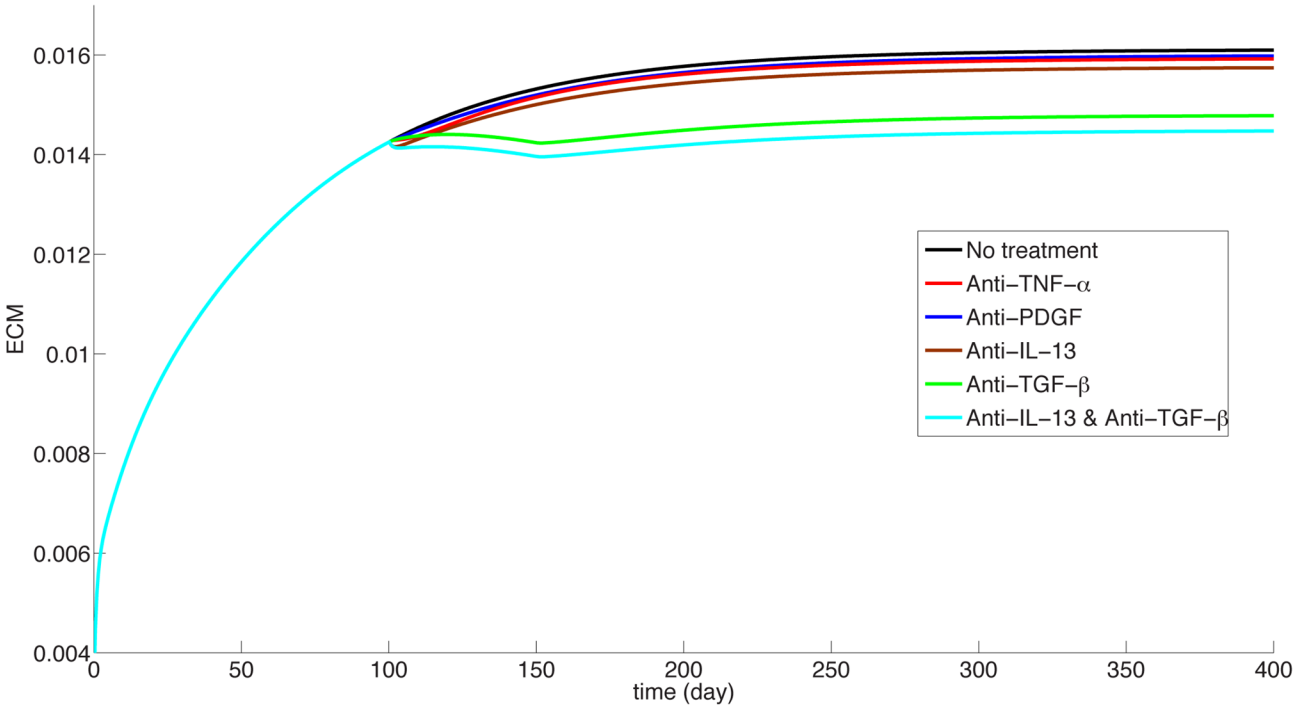

Fig 7. Treatment studies for the mild case. ECM is in units of gm/cm^3.

doi:10.1371/journal.pone.0135097.g007

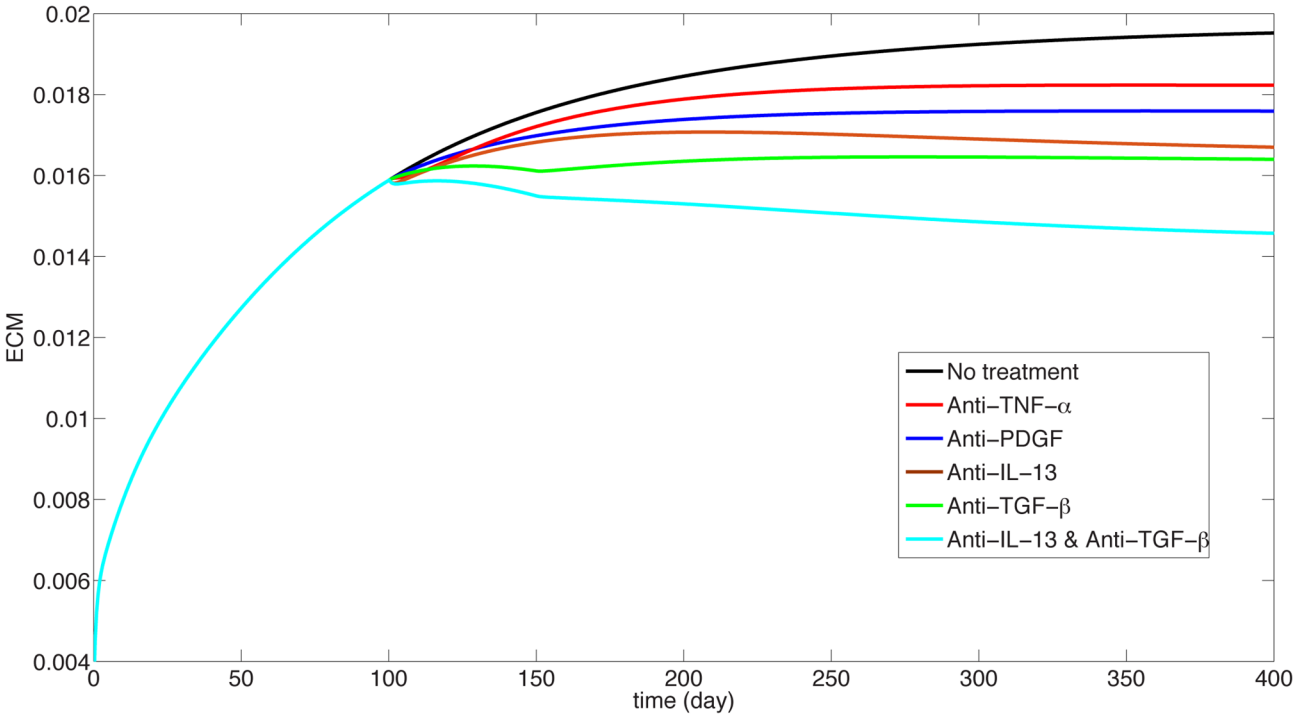

Fig 8. Treatment studies for the severe case. ECM is in units of gm/cm^3.

doi:10.1371/journal.pone.0135097.g008

We can use the model to explore novel therapeutic approaches to the treatment of IPF. For example, what will be the effect of combining two anti-fibrotic drugs? From Figs 5 and 7 we see that anti-TGF-β is the most effective drug to slow the IPF progression (with $A = B = 0.1$) and anti-IL-13 has only very mild benefits (with $B_3 = 1$). However if we combine these two drugs (at the same respective levels) we obtain significant improvement of over anti-TGF-β alone, especially in the case of severe case of IPF, as seen in the bottom curves in Figs 5 and 7. We propose this result as an hypothesis that could be checked in clinical trials.

The present model should be viewed as a first step in the development a more comprehensive study of IPF. Such a study should include altered DNA methylation [47, 48], epigenetic and environmental factors [49], gene mutation (e.g. of surfactant protein [50]), polymorphism (e.g. of IL-10 [51], IL-4 [52], Muc5B [53]), and telomerase mutations [54].

Acknowledgments

This research has been supported by the Mathematical Biosciences Institute and the National Science Foundation under Grant DMS 0931642.

Author Contributions

Conceived and designed the experiments: WH CM AF. Analyzed the data: WH CM AF. Wrote the paper: WH CM AF.

References

1. Selman M, Pardo A. Revealing the pathogenic and aging-related mechanisms of the enigmatic idiopathic pulmonary fibrosis. an integral model. Am J Respir Crit Care Med. 2014 May; 189(10):1161–1172. doi: 10.1164/rccm.201312-2221PP PMID: 24641682
2. Bargagli E, Prasse A, Olivieri C, Muller-Quernheim J, Rottoli P. Macrophage-derived biomarkers of idiopathic pulmonary fibrosis. Pulm Med. 2011; 2011:717130. doi: 10.1155/2011/717130 PMID: 21637368
3. W NP. Epithelial fibroblast triggering and interactions in pulmonary fibrosis. Eur Respir Rev. 2008 May; 17(109):123–129. doi: 10.1183/09059180.00010904
4. Daniil ZD, Papageorgiou E, Koutsokera A, Kostikas K, Kiropoulos T, Papaioannou AI, et al. Serum levels of oxidative stress as a marker of disease severity in idiopathic pulmonary fibrosis. Pulm Pharmacol Ther. 2008; 21(1):26–31. doi: 10.1016/j.pupt.2006.10.005 PMID: 17161968
5. Kliment CR, Oury TD. Oxidative stress, extracellular matrix targets, and idiopathic pulmonary fibrosis. Free Radic Biol Med. 2010 Sep; 49(5):707–717. doi: 10.1016/j.freeradbiomed.2010.04.036 PMID: 20452419
6. Camelo A, Dunmore R, Sleeman MA, Clarke DL. The epithelium in idiopathic pulmonary fibrosis: breaking the barrier. Front Pharmacol. 2014 Jan; 4:173. doi: 10.3389/fphar.2013.00173 PMID: 24454287
7. Herzog EL, Bucala R. Fibrocytes in health and disease. Exp Hematol. 2010 Jul; 38(7):548–556. doi: 10.1016/j.exphem.2010.03.004 PMID: 20303382
8. Malli F, Koutsokera A, Paraskeva E, Zakynthinos E, Papagianni M, Makris D, et al. Endothelial progenitor cells in the pathogenesis of idiopathic pulmonary fibrosis: an evolving concept. PLoS ONE. 2013; 8 (1):e53658. doi: 10.1371/journal.pone.0053658 PMID: 23341966
9. Bringardner BD, Baran CP, Eubank TD, Marsh CB. The role of inflammation in the pathogenesis of idiopathic pulmonary fibrosis. Antioxid Redox Signal. 2008 Feb; 10(2):287–301. doi: 10.1089/ars.2007.1897 PMID: 17961066
10. Homer RJ, Elias JA, Lee CG, Herzog E. Modern concepts on the role of inflammation in pulmonary fibrosis. Arch Pathol Lab Med. 2011 Jun; 135(6):780–788. PMID: 21631273
11. Zoz DF, Lawson WE, Blackwell TS. Idiopathic pulmonary fibrosis: a disorder of epithelial cell dysfunction. Am J Med Sci. 2011 Jun; 341(6):435–438. doi: 10.1097/MAJ.0b013e31821a9d8e PMID: 21613930
12. Boorsma CE, Draijer C, Melgert BN. Macrophage heterogeneity in respiratory diseases. Mediators Inflamm. 2013; 2013:769214. doi: 10.1155/2013/769214 PMID: 23533311

13. McRitchie DI, Isowa N, Edelson JD, Xavier AM, Cai L, et al. Production of tumour necrosis factor alpha by primary cultured rat alveolar epithelial cells. Cytokine. 2000 Jun; 12(6):644–654. doi: 10.1006/cyto.1999.0656 PMID: 10843740

14. Iyonaga K, Takeya M, Saita N, Sakamoto O, Yoshimura T, Ando M, et al. Monocyte chemoattractant protein-1 in idiopathic pulmonary fibrosis and other interstitial lung diseases. Hum Pathol. 1994 May; 25 (5):455–463. doi: 10.1016/0046-8177(94)90117-1 PMID: 8200639

15. Selman M, Pardo A. Role of epithelial cells in idiopathic pulmonary fibrosis: from innocent targets to serial killers. Proc Am Thorac Soc. 2006 Jun; 3(4):364–372. doi: 10.1513/pats.200601-003TK PMID: 16738202

16. Landsman L, Jung S. Lung macrophages serve as obligatory intermediate between blood monocytes and alveolar macrophages. J Immunol. 2007 Sep; 179(6):3488–3494. doi: 10.4049/jimmunol.179.6.3488 PMID: 17785782

17. Stahl M, Schupp J, Jager B, Schmid M, Zissel G, Muller-Quernheim J, et al. Lung collagens perpetuate pulmonary fibrosis via CD204 and M2 macrophage activation. PLoS ONE. 2013; 8(11):e81382. doi: 10.1371/journal.pone.0081382 PMID: 24278429

18. Pechkovsky DV, Prasse A, Kollert F, Engel KM, Dentler J, Luttmann W, et al. Alternatively activated alveolar macrophages in pulmonary fibrosis-mediator production and intracellular signal transduction. Clin Immunol. 2010 Oct; 137(1):89–101. doi: 10.1016/j.clim.2010.06.017 PMID: 20674506

19. Kuwano K, Hagimoto N, Nakanishi Y. The role of apoptosis in pulmonary fibrosis. Histol Histopathol. 2004 Jul; 19(3):867–881. PMID: 15168350

20. Sakai N, Tager AM. Fibrosis of two: Epithelial cell-fibroblast interactions in pulmonary fibrosis. Biochim Biophys Acta. 2013 Jul; 1832(7):911–921. doi: 10.1016/j.bbadis.2013.03.001 PMID: 23499992

21. Redente EF, Keith RC, Janssen W, Henson PM, Ortiz LA, Downey GP, et al. Tumor necrosis factor-alpha accelerates the resolution of established pulmonary fibrosis in mice by targeting profibrotic lung macrophages. Am J Respir Cell Mol Biol. 2014 Apr; 50(4):825–837. doi: 10.1165/rcmb.2013-0386OC PMID: 24325577

22. Clarke DL, Carruthers AM, Mustelin T, Murray LA. Matrix regulation of idiopathic pulmonary fibrosis: the role of enzymes. Fibrogenesis Tissue Repair. 2013; 6(1):20. doi: 10.1186/1755-1536-6-20 PMID: 24279676

23. Fichtner-Feigl S, Strober W, Kawakami K, Puri RK, Kitani A. IL-13 signaling through the IL-13alpha2 receptor is involved in induction of TGF-beta1 production and fibrosis. Nat Med. 2006 Jan; 12(1):99–106. doi: 10.1038/nm1332 PMID: 16327802

24. Jakubzick C, Choi ES, Joshi BH, Keane MP, Kunkel SL, Puri RK, et al. Therapeutic attenuation of pulmonary fibrosis via targeting of IL-4- and IL-13-responsive cells. J Immunol. 2003 Sep; 171(5):2684–2693. doi: 10.4049/jimmunol.171.5.2684 PMID: 12928422

25. Vasakova M, Striz I, Slavcev A, Jandova S, Kolesar L, Sulc J. Th1/Th2 cytokine gene polymorphisms in patients with idiopathic pulmonary fibrosis. Tissue Antigens. 2006 Mar; 67(3):229–232. doi: 10.1111/j.1399-0039.2006.00560.x PMID: 16573560

26. Gharib SA, Johnston LK, Huizar I, Birkland TP, Hanson J, Wang Y, et al. MMP28 promotes macrophage polarization toward M2 cells and augments pulmonary fibrosis. J Leukoc Biol. 2014 Jan; 95 (1):9–18. doi: 10.1189/jlb.1112587 PMID: 23964118

27. Lomas NJ, Watts KL, Akram KM, Forsyth NR, Spiteri MA. Idiopathic pulmonary fibrosis: immunohistochemical analysis provides fresh insights into lung tissue remodelling with implications for novel prognostic markers. Int J Clin Exp Pathol. 2012; 5(1):58–71. PMID: 22295148

28. Murray LA, Chen Q, Kramer MS, Hesson DP, Argentieri RL, Peng X, et al. TGF-beta driven lung fibrosis is macrophage dependent and blocked by Serum amyloid P. Int J Biochem Cell Biol. 2011 Jan; 43 (1):154–162. doi: 10.1016/j.biocel.2010.10.013

29. Tatler AL, Jenkins G. TGF-beta activation and lung fibrosis. Proc Am Thorac Soc. 2012 Jul; 9(3):130–136. doi: 10.1513/pats.201201-003AW PMID: 22802287

30. Xiao L, Du Y, Shen Y, He Y, Zhao H, Li Z. TGF-beta 1 induced fibroblast proliferation is mediated by the FGF-2/ERK pathway. Front Biosci (Landmark Ed). 2012; 17:2667–2674. doi: 10.2741/4077

31. Ulrich D, Ulrich F, Unglaub F, Piatkowski A, Pallua N. Matrix metalloproteinases and tissue inhibitors of metalloproteinases in patients with different types of scars and keloids. J Plast Reconstr Aesthet Surg. 2010 Jun; 63(6):1015–1021. doi: 10.1016/j.bjps.2009.04.021 PMID: 19464975

32. Hao W, Rovin BH, Friedman A. Mathematical model of renal interstitial fibrosis. Proc Natl Acad Sci USA. 2014 Sep; 111(39):14193–14198. doi: 10.1073/pnas.1413970111 PMID: 25225370

33. Ochs M, Nyengaard JR, Jung A, Knudsen L, Voigt M, Wahlers T, et al. The number of alveoli in the human lung. Am J Respir Crit Care Med. 2004 Jan; 169(1):120–124. doi: 10.1164/rccm.200308-1107OC

34. Xue C, Friedman A, Sen CK. A mathematical model of ischemic cutaneous wounds. Proc Natl Acad Sci USA. 2009 Sep; 106(39):16782–16787. doi: 10.1073/pnas.0909115106 PMID: 19805373

35. Park SW, Ahn MH, Jang HK, Jang AS, Kim DJ, Koh ES, et al. Interleukin-13 and its receptors in idiopathic interstitial pneumonia: clinical implications for lung function. J Korean Med Sci. 2009 Aug; 24 (4):614–620. doi: 10.3346/jkms.2009.24.4.614 PMID: 19654941

36. Orbe J, Rodriguez JA, Arias R, Belzunce M, Nespereira B, Perez-Ilzarbe M, et al. Antioxidant vitamins increase the collagen content and reduce MMP-1 in a porcine model of atherosclerosis: implications for plaque stabilization. Atherosclerosis. 2003 Mar; 167(1):45–53. doi: 10.1016/S0021-9150(02)00392-1 PMID: 12618267

37. Mann CJ, Perdiguero E, Kharraz Y, Aguilar S, Pessina P, Serrano AL, et al. Aberrant repair and fibrosis development in skeletal muscle. Skelet Muscle. 2011; 1(1):21. doi: 10.1186/2044-5040-1-21 PMID: 21798099

38. Jikov VV, Kozlov SM, Oleinik OA. Homogenization of differential operators and integral functionals. Springer-Verlag. 1994;.

39. Crouser ED, Culver DA, Knox KS, Julian MW, Shao G, Abraham S, et al. Gene expression profiling identifies MMP-12 and ADAMDEC1 as potential pathogenic mediators of pulmonary sarcoidosis. Am J Respir Crit Care Med. 2009 May; 179(10):929–938. doi: 10.1164/rccm.200803-490OC PMID: 19218196

40. Hao W, Crouser ED, Friedman A. Mathematical model of sarcoidosis. Proc Natl Acad Sci USA. 2014 Nov; 111(45):16065–16070. doi: 10.1073/pnas.1417789111 PMID: 25349384

41. Nkyimbeng T, Ruppert C, Shiomi T, Dahal B, Lang G, Seeger W, et al. Pivotal role of matrix metalloproteinase 13 in extracellular matrix turnover in idiopathic pulmonary fibrosis. PLoS ONE. 2013; 8(9): e73279. doi: 10.1371/journal.pone.0073279 PMID: 24023851

42. Bergeron A, Soler P, Kambouchner M, Loiseau P, Milleron B, Valeyre D, et al. Cytokine profiles in idiopathic pulmonary fibrosis suggest an important role for TGF-beta and IL-10. Eur Respir J. 2003 Jul; 22 (1):69–76. doi: 10.1183/09031936.03.00014703 PMID: 12882453

43. Cho JH, Gelinas R, Wang K, Etheridge A, Piper MG, Batte K, et al. Systems biology of interstitial lung diseases: integration of mRNA and microRNA expression changes. BMC Med Genomics. 2011; 4:8. doi: 10.1186/1755-8794-4-8 PMID: 21241464

44. Raghu G, Brown KK, Costabel U, Cottin V, du Bois RM, Lasky JA, et al. Treatment of idiopathic pulmonary fibrosis with etanercept: an exploratory, placebo-controlled trial. Am J Respir Crit Care Med. 2008 Nov; 178(9):948–955. doi: 10.1164/rccm.200709-1446OC PMID: 18669816

45. Daniels CE, Lasky JA, Limper AH, Mieras K, Gabor E, Schroeder DR, et al. Imatinib treatment for idiopathic pulmonary fibrosis: Randomized placebo-controlled trial results. Am J Respir Crit Care Med. 2010 Mar; 181(6):604–610. doi: 10.1164/rccm.200906-0964OC PMID: 20007927

46. Takeda Y, Tsujino K, Kijima T, Kumanogoh A. Efficacy and safety of pirfenidone for idiopathic pulmonary fibrosis. Patient Prefer Adherence. 2014; 8:361–370. doi: 10.2147/PPA.S37233 PMID: 24711695

47. Sanders YY, Ambalavanan N, Halloran B, Zhang X, Liu H, et al. Altered DNA methylation profile in idiopathic pulmonary fibrosis. Am J Respir Crit Care Med. 2012 Sep; 186(6):525–535. doi: 10.1164/rccm.201201-0077OC PMID: 22700861

48. Rabinovich EI, Kapetanaki MG, Steinfeld I, Gibson KF, Pandit KV, Yu G, et al. Global methylation patterns in idiopathic pulmonary fibrosis. PLoS ONE. 2012; 7(4):e33770. doi: 10.1371/journal.pone.0033770 PMID: 22506007

49. Yang IV, Schwartz DA. Epigenetics of idiopathic pulmonary fibrosis. Transl Res. 2015 Jan; 165(1):48–60. doi: 10.1016/j.trsl.2014.03.011 PMID: 24746870

50. Nogee LM, Dunbar AE, Wert S, Askin F, Hamvas A, Whitsett JA. Mutations in the surfactant protein C gene associated with interstitial lung disease. Chest. 2002 Mar; 121(3 Suppl):20S–21S. doi: 10.1378/chest.121.3_suppl.20S PMID: 11893657

51. Whittington HA, Freeburn RW, Godinho SI, Egan J, Haider Y, Millar AB. Analysis of an IL-10 polymorphism in idiopathic pulmonary fibrosis. Genes Immun. 2003 Jun; 4(4):258–264. doi: 10.1038/sj.gene.6363959 PMID: 12761561

52. Vasakova M, Sterclova M, Matej R, Olejar T, Kolesar L, Skibova J, et al. IL-4 polymorphisms, HRCT score and lung tissue markers in idiopathic pulmonary fibrosis. Hum Immunol. 2013 Oct; 74(10):1346–1351. doi: 10.1016/j.humimm.2013.07.011 PMID: 23911740

53. Seibold MA, Wise AL, Speer MC, Steele MP, Brown KK, et al. A common MUC5B promoter polymorphism and pulmonary fibrosis. N Engl J Med. 2011 Apr; 364(16):1503–1512. doi: 10.1056/NEJMoa1013660 PMID: 21506741

54. Armanios M. Telomerase mutations and the pulmonary fibrosis-bone marrow failure syndrome complex. N Engl J Med. 2012 Jul; 367(4):384; author reply 384. doi: 10.1056/NEJMc1206730 PMID: 22830481

55. Hao W, Friedman A. The LDL-HDL Profile Determines the Risk of Atherosclerosis: A Mathematical Model. PLoS ONE. 2014; 9(3):e90497. doi: 10.1371/journal.pone.0090497 PMID: 24621857

56. Day J, Friedman A, Schlesinger LS. Modeling the immune rheostat of macrophages in the lung in response to infection. Proc Natl Acad Sci USA. 2009 Jul; 106(27):11246–11251. doi: 10.1073/pnas.0904846106 PMID: 19549875

57. Alleva DG, Burger CJ, Elgert KD. Tumor-induced regulation of suppressor macrophage nitric oxide and TNF-alpha production. Role of tumor-derived IL-10, TGF-beta, and prostaglandin E2. J Immunol. 1994 Aug; 153(4):1674–1686. PMID: 8046239

58. Murphy J, Summer R, Wilson AA, Kotton DN, Fine A. The prolonged life-span of alveolar macrophages. Am J Respir Cell Mol Biol. 2008 Apr; 38(4):380–385. doi: 10.1165/rcmb.2007-0224RC PMID: 18192503

59. Oliver JC, Bland LA, Oettinger CW, Arduino MJ, McAllister SK, Aguero SM, et al. Cytokine kinetics in an in vitro whole blood model following an endotoxin challenge. Lymphokine Cytokine Res. 1993 Apr; 12(2):115–120. PMID: 8324076